include the "lab-on-a-chip" concept. The robots could be used for multistation single-cell diagnostics. The robot arm could arrest biological entities (single cells, bacteria, multicellular organisms, etc.) from a sample and then transfer them sequentially to different measurement stations of a multisensor area, as demonstrated by the transfer of the glass bead over the tracks. An array of standing microrobots, whose fingers are treated with adhesion molecules, could be used to select given cells or bacteria in a sample and then transfer them to the multisensor area. The testing could also be done by small additional structures on the microrobot itself, such as extra electrodes for electrical measurements. The electrodes could also be located on the chip itself, for example, in microvials, which also enable single-cell chemical modifications.

A nonbiomedical application for microrobots is the assembly of microstructures in a so-called "factory on a desk." The microrobot could be used to assemble other microstructures. Most of this is still done manually, which is cumbersome, time-consuming, and expensive. Small micromachined conveyors for this purpose have already been demonstrated (*18, 19*). An advantage of assembly in water could be the reduction of gravitational forces and slow diffusion constants of the objects to assemble. The robot could assist the self-assembly (*20*).

Design for the manipulation of cells will require choosing the proper dimensions of the microrobot. The simple scalability of the presented robots—they can easily be reduced in lateral dimension by one order of magnitude—is an important advantage. Also, our microactuators can be seen as active hinges, where only one electrical contact is needed per element, reducing the amount of dead area on the chip. This leads to the possibility of a large number of parallel-operated microrobots on a small area for the simultaneous handling of a large number of cells. Electrostatically operated microactuators require a considerable area for ingenious but complex systems using comb drive actuators and push or pull rods to rotate a plate out of the surface plane. To extend the range of the robot, some modifications of the present design should be made, like adding a rotating base. Using on-chip counter and working electrodes (*21*) would truly integrate the robot into a microelectromechanical system. The operation of such devices may enable new methods in biotechnology.

References and Notes

1. G. Fuhr and S. G. Shirley, *J. Micromech. Microeng.* **5**, 77 (1995).
2. R. Yeh, E. J. J. Kruglick, K. S. J. Pister, *J. Microelectromech. Syst.* **5**, 10 (1996).
3. K. Suzuki, I. Shimoyama, H. Miura, *J. Microelectromech. Syst.* **3**, 4 (1994).
4. C.-J. Kim, A. P. Pisano, R. S. Muller, *J. Microelectromech. Syst.* **1**, 31 (1992).
5. T. Ebefors, J. U. Mattsson, E. Kälvesten, G. Stemme, in *The 10th International Conference on Solid-State Sensors and Actuators, Digest of Technical Papers*, M. Esashi, Ed. (Institute of Electrical Engineers of Japan, Tokyo, 1999), pp. 1202–1205.
6. R. H. Baughman, L. W. Shacklette, R. L. Elsenbaumer, E. J. Plichta, C. Becht, in *Molecular Electronics*, P. I. Lazarev, Ed. (Kluwer Academic, Dordrecht, Netherlands, 1991), pp. 267–289.
7. T. F. Otero and J. M. Sansinena, *Proc. SPIE Int. Soc. Opt. Eng.* **2779**, 365 (1996).
8. A. Della Santa, D. De Rossi, A. Mazzoldi, *Smart Mater. Struct.* **6**, 23 (1997).
9. M. R. Gandhi, P. Murray, G. M. Spinks, G. G. Wallace, *Synth. Met.* **73**, 247 (1995).
10. Q. Pei and O. Inganäs, *Adv. Mater.* **4**, 277 (1992).
11. E. Smela, O. Inganäs, Q. Pei, I. Lundström, *Adv. Mater.* **5**, 630 (1993).
12. E. Smela, O. Inganäs, I. Lundström, *Science* **268**, 1735 (1995).
13. E. W. H. Jager, E. Smela, O. Inganäs, I. Lundström, *Proc. SPIE Int. Soc. Opt. Eng.* **3669**, 377 (1999).
14. E. Smela, *J. Micromech. Microeng.* **9**, 1 (1999).
15. ———, O. Inganäs, I. Lundström, in *The 8th International Conference on Solid-State Sensors and Actuators, and Eurosensors IX, Digest of Technical Papers* (Royal Swedish Academy of Engineering Sciences, Stockholm, 1995), pp. 218–219.
16. A film showing the full movement of this sequence and other actuations of the robotic arm is available at www.sciencemag.org/feature/data/1050465.shl.
17. Y. Xia and G. M. Whitesides, *Angew. Chem. Int. Ed. Engl.* **37**, 550 (1998).
18. H. Nakazawa *et al.*, in *The 10th International Conference on Solid-State Sensors and Actuators, Digest of Technical Papers*, M. Esashi, Ed. (Institute of Electrical Engineers of Japan, Tokyo, 1999), pp. 1192–1195.
19. Y. Mita, T. Oba, M. Mita, G. Hashiguchi, H. Fujita, in *The 10th International Conference on Solid-State Sensors and Actuators, Digest of Technical Papers*, M. Esashi, Ed. (Institute of Electrical Engineers of Japan, Tokyo, 1999), pp. 1196–1197.
20. T. L. Breen, J. Tien, S. R. J. Oliver, T. Hadzic, G. M. Whitesides, *Science* **284**, 948 (1999).
21. E. W. H. Jager, E. Smela, O. Inganäs, *Sens. Actuators B Chem.* **56**, 73 (1999).

22. E.W.H.J. is a Ph.D. student in the graduate school Forum Scientum and thanks the Swedish Foundation for Strategic Research (SSF) for its financial support. The micromuscle project is supported by the Swedish Research Council for Engineering Sciences (TFR).

16 March 2000; accepted 2 May 2000

Fractional Quantum Hall Effect in Organic Molecular Semiconductors

J. H. Schön, Ch. Kloc, B. Batlogg

High-quality crystals of the organic molecular semiconductors tetracene and pentacene were used to prepare metal-insulator-semiconductor (MIS) structures exhibiting hole and electron mobilities exceeding 10^4 square centimeters per volt per second. The carrier concentration in the channel region of these ambipolar field-effect devices was controlled by the applied gate voltage. Well-defined Shubnikov–de Haas oscillations and quantized Hall plateaus were observed for two-dimensional carrier densities in the range of 10^{11} per square centimeter. Fractional quantum Hall states were observed in tetracene crystals at temperatures as high as ~2 kelvin.

The quantum Hall effect (QHE) (*1*), in which the Hall resistance R_{xy} of a quasi–two-dimensional (2D) electron or hole gas becomes quantized with values $R_{xy} = h/e^2j$ (where h is Planck's constant, e is the electron charge, and j is an integer), has been observed in a variety of inorganic semiconductors, such as Si, GaAs, InAs, and InP. At higher magnetic fields, fractional quantum Hall states where j is not an integer have also been observed (*2*). A QHE-like state was also seen in organic materials such as Bechgaard salts $(TMTSF)_2X$ (where TMTSF is tetramethyl tetraselenafulvalene and X = ClO_4, ReO_4, or PF_6) (*3–5*). However, in these materials the QHE is related to a series of field-induced spin density wave transitions (*5*) to states with filled Landau bands (*6*). We report on the observation of the integer and fractional QHE in a 2D electron and hole gas in the organic semiconductors tetracene and pentacene. This was achieved in a 2D electron-hole system generated in a single crystal–based MIS device.

Bell Laboratories, Lucent Technologies, 600 Mountain Avenue, Murray Hill, NJ 07974, USA.

Pentacene and tetracene single crystals were grown from the vapor phase in a stream of flowing gas (*7, 8*). The resulting high-quality single crystals support ambipolar (i.e., electron and hole) transport (*9*). Thermally evaporated gold films provide ohmic contacts for holes as well as electrons. Because these crystals are of high resistivity (>10^{14} ohm·cm), the charge carriers must be injected in a field-effect transistor geometry, in which an Al_2O_3 layer (capacitance ~130 nF cm^{-2}) serves as the gate dielectric. A thin gold layer is deposited as the gate electrode on top of the structure. We can then produce a 2D electron or hole gas, respectively, in the channel region of an organic field-effect transistor (*10*), with the carrier density controlled by the gate bias.

The charge transport properties in these structures were studied down to 1.7 K in magnetic fields up to 9 T by dc measurements in a conventional six-point Hall geometry (Quantum Design physical properties measurement system). A plot of the charge carrier mobility μ as a function of temperature for concentrations of $\sim 10^{11}$ carriers cm^{-2} (Fig. 1) shows that values as high as 10^5 cm^2 V^{-1} s^{-1} are achieved in MIS devices. These electron and hole mobility values are much higher than in earlier generations of crystals on which we had fabricated ambipolar field-effect transistors (*9*). We ascribe this mobility improvement at low temperatures to additional purification and optimization of the growth conditions. Note that the mobilities at higher temperatures remain unchanged, reflecting the intrinsic nature of these high-temperature values (e.g., at room temperature, $\mu_{RT} \approx 3$ cm^2 V^{-1} s^{-1} for holes in pentacene).

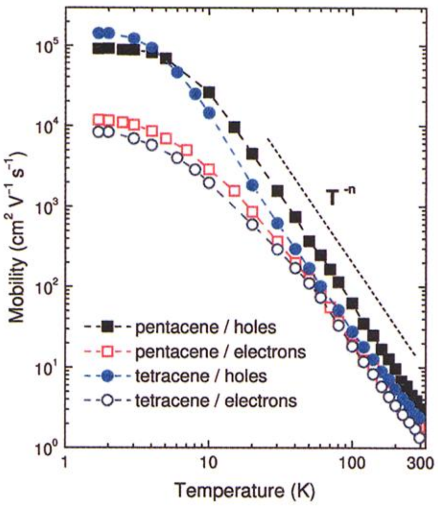

Fig. 1. Charge carrier mobility in pentacene and tetracene as a function of temperature.

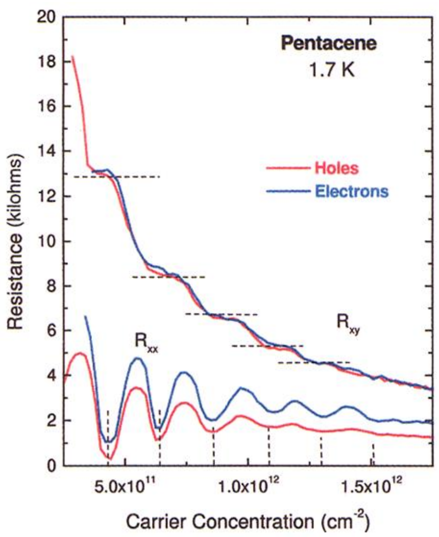

Fig. 2. Magnetoresistance and Hall resistance as function of electron and hole concentration in a pentacene MIS device at 1.7 K. Distinct Hall plateaus and well-pronounced magnetoresistance oscillations are clearly visible.

The approximate power law dependence of the mobility on temperature ($\propto T^{-n}$, where $n \approx 2.5$ to 2.7) was recognized as the intrinsic property of polyacene single crystals and is ascribed to electron-phonon interaction (*9*, *11*). However, at low temperatures (<10 K), charged point defects seem to limit the mobility (*12*). Hence, careful preparation and purification are prerequisites to obtain mobilities exceeding 10^4 cm^2 V^{-1} s^{-1} in this class of materials.

The magnetoresistance R_{xx} and the Hall resistance R_{xy} at 1.7 K at a fixed magnetic field of 9 T in a single crystalline pentacene MIS device are shown in Fig. 2 as a function of electron and hole density in the transistor channel. Well-pronounced oscillations (Shubnikov–de Haas effect) and Hall plateaus are observed. The Hall plateaus are quantized with $R_{xy} = h/je^2$ (j integer) corresponding to the integer QHE in a 2D electron gas (*1*, *13*). Moreover, the oscillations and plateaus are observed for both electrons and holes in the same sample. Hall plateaus are clearly visible for filling factors $j = 2$ to $j = 6$, and less pronounced structures can be found in R_{xy} up to $j = 10$ (Fig. 3). The effective hole mass m^* can be determined from the temperature-dependent amplitude of the Shubnikov–de Haas oscillations (Fig. 3). We derived values of 1.55 ± 0.2 m_e and 1.3 ± 0.3 m_e (where m_e is the free electron mass) for holes in pentacene and tetracene, respectively. Assuming a cosine-shaped band dispersion and neglecting the in-plane anisotropy, an effective electronic bandwidth W of ~ 0.5 eV can be estimated from this effective mass. This is similar to theoretical estimates based on either local density approximation (*14*) or quantum chemical cluster calculations (*15*), but is much larger than in earlier calculations (*16*, *17*) or estimates based on extended Hückel calculations (*18*).

We observed the most striking results in crystals of tetracene with a low-temperature hole mobility of $\sim 10^5$ cm^2 V^{-1} s^{-1}. By changing the gate voltage, we swept the 2D hole concentration from 0.5 to 5×10^{11} cm^{-2} and simultaneously measured the resistance and Hall voltage. The quantization of both R_{xx} and R_{xy} is well developed (Fig. 4), and the low density renders all the integer quantum Hall states accessible up to $j = 1$. At low densities ($<7 \times 10^{10}$ cm^{-2}), we can resolve the fractional quantum Hall state $j = 1/3$ and a less pronounced $j = 2/3$, as well as $j = 2/5$ (Fig. 5). This observation is remarkable because it occurs at a relatively high temperature of 1.7 K. This is, however, not too surprising when we consider that the scattering time τ ($\tau = m^*\mu/e$) in our samples ($\mu \approx 10^5$ cm^2 V^{-1} s^{-1}, $m^* \approx 1.5 m_e$) is as long as in high-quality GaAs

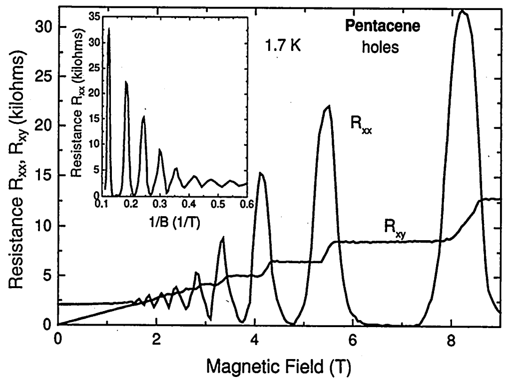

Fig. 3. Shubnikov–de Haas oscillations and quantum Hall plateaus in pentacene at 1.7 K. The hole concentration is 4×10^{11} cm^{-2}. The inset shows the oscillations of the magnetoresistance R_{xx} as function of reciprocal magnetic field. An effective hole mass of $1.55 m_e$ is deduced from the temperature dependence of the amplitude of the R_{xx} oscillations.

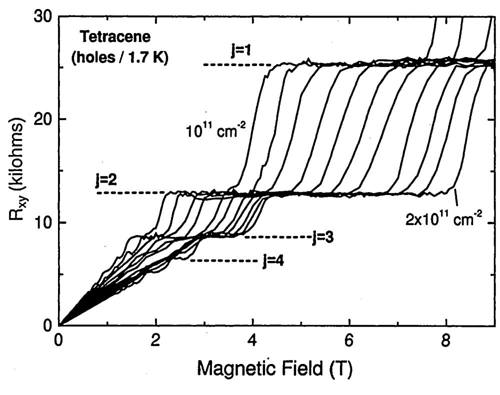

Fig. 4. Hall resistance for different hole concentrations from 10^{11} to 2×10^{11} cm^{-2} in a tetracene MIS device at 1.7 K (step of 10^{10} cm^{-2}). Distinct integer Hall plateaus are observed.

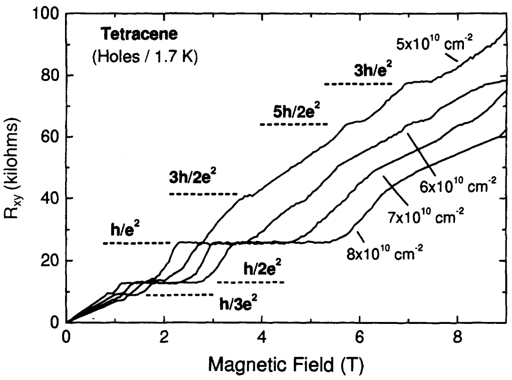

Fig. 5. Hall resistance for low hole concentration (5×10^{10} to 8×10^{10} cm^{-2}) in a tetracene MIS device at 1.7 K. Distinct integer Hall plateaus and the fractional quantum Hall states $j = 1/3$, $j = 2/3$, and $j = 2/5$ are clearly visible.

samples with mobilities of several million square centimeters per volt per second. In addition, the combination of a reduced dielectric constant and a much higher effective mass than in GaAs makes new parameter regions accessible, enabling studies of the physics of strongly interacting electron systems, such as the metal-insulator transition in two dimensions (*19*).

We have presented ample experimental evidence for band-like charge transport in delocalized states in these organic semiconductors: the high mobilities observed at low temperatures, the temperature dependence of the mobility, the large effective bandwidth at low temperatures ($W \gg k_B T$, where k_B is the Boltzmann constant), Shubnikov–de Haas oscillations, and the observation of the integer and fractional QHE. All these observations of transport properties, particularly at low temperatures, are similar to those observed in conventional inorganic semiconductors. It appears that the measured effective masses of order 1 to 1.5 m_e are not those of bare holes or electrons, but instead are charge carriers dressed by a polarization cloud. Looking forward, then, one might expect the adoption of additional concepts from inorganic semiconductor technology (such as superlattices and quantum wells) to yield interesting electronic and optical properties. Layered organic semiconductors (*17, 19, 20*) could offer more latitude for device engineering because they are van der Waals–bonded, and hence minimal constraints are imposed by lattice matching (*21, 22*). Furthermore, interesting new phenomena can be anticipated to result from stronger electron-phonon interaction or strong transport anisotropy, opening up a new field of research.

References and Notes

1. K. von Klitzing, G. Dorda, M. Pepper, *Phys. Rev. Lett.* **45**, 494 (1980).
2. H. L. Stormer, *Rev. Mod. Phys.* **71**, 875 (1999); D. C. Tsui, H. L. Stormer, A. C. Gossard, *Phys. Rev. B* **25**, 1408 (1982).
3. M. Ribault *et al.*, *J. Phys. Lett.* **45**, L935 (1984).
4. R. V. Chamberlin *et al.*, *Phys. Rev. Lett.* **60**, 1189 (1988).
5. P. M. Chaikin, W. Kang, S. Hannahs, R. C. Yu, *Physica B* **177**, 353 (1992).
6. For another organic system, α-(BEDT-TTF)$_2$MHg-(SCN)$_4$ salts [where BEDT-TTF is bis(ethylenedithio)-tetrathiafulvalene and M = K or Tl], indirect evidence of a QHE was found in high-field de Haas–van Alphen measurements; this was supported by further evidence from Hall transport measurements. These phenomena in charge-transfer salts, however, are ascribed to a bulk QHE substantially different from the "conventional" QHE in a 2D electron gas in an inorganic heterostructure or in a MIS structure [N. Harrison *et al.*, *Phys. Rev. Lett.* **77**, 1576 (1996); M. M. Honold *et al.*, *Phys. Rev. B* **59**, R10417 (1999)].
7. Ch. Kloc, P. G. Simpkins, T. Siegrist, R. A. Laudise, *J. Cryst. Growth* **182**, 416 (1997).
8. R. A. Laudise, Ch. Kloc, P. G. Simpkins, T. Siegrist, *J. Cryst. Growth* **187**, 449 (1998).
9. J. H. Schön, S. Berg, Ch. Kloc, B. Batlogg, *Science* **287**, 1022 (2000).
10. A. Dodabalapur, L. Torsi, H. E. Katz, *Science* **268**, 270 (1995).
11. N. Karl, J. Marktanner, R. Stehle, W. Warta, *Synth. Met.* **41–43**, 2473 (1991).
12. D. M. Burland and U. Konzelmann, *J. Chem. Phys.* **67**, 319 (1977).
13. K. von Klitzing, *Rev. Mod. Phys.* **58**, 519 (1986).
14. P. M. Littlewood, personal communication.
15. J. Cornil, personal communication.
16. W. Warta and N. Karl, *Phys. Rev. B* **32**, 1172 (1985).
17. D. C. Singh and S. C. Matur, *Mol. Cryst. Liq. Cryst.* **27**, 55 (1974).
18. R. C. Haddon, personal communication.
19. S. V. Kravchenko, G. V. Kravchenko, J. E. Furneaux, V. M. Pudalov, M. D'Iorio, *Phys. Rev. B* **50**, 8039 (1994).
20. H. Akimichi, T. Inoshita, S. Hotta, H. Noge, H. Sakaki, *Appl. Phys. Lett.* **63**, 3158 (1993).
21. T. Minakata and Y. Mori, *Pol. Adv. Technol.* **6**, 611 (1995).
22. F. F. So and S. R. Forrest, *Phys. Rev. Lett.* **66**, 2649 (1991).

23. We thank E. Bucher for use of his equipment, and A. Dodabalapur, J. W. P. Hsu, H. Y. Hwang, H. L. Störmer, and C. M. Varma for helpful discussions. Supported by the Deutsche Forschungsgemeinschaft (J.H.S.).

6 April 2000; accepted 19 May 2000

Discovery of a High-Energy Gamma-Ray–Emitting Persistent Microquasar

Josep M. Paredes,[1]* Josep Martí,[2] Marc Ribó,[1] Maria Massi[3]

Microquasars are stellar x-ray binaries that behave as a scaled-down version of extragalactic quasars. The star LS 5039 is a new microquasar system with apparent persistent ejection of relativistic plasma at a 3-kiloparsec distance from the sun. It may also be associated with a γ-ray source discovered by the Energetic Gamma Ray Experiment Telescope (EGRET) on board the COMPTON–Gamma Ray Observatory satellite. Before the discovery of LS 5039, merely a handful of microquasars had been identified in the Galaxy, and none of them was detected in high-energy γ-rays.

The $V = 11.2$ magnitude star LS 5039 (*1*) has been recently identified as a nearby high-mass x-ray binary with spectral type O7V((f)) (*2*) and persistent radio emission (*3, 4*). Here, we report high-resolution radio observations with the Very Long Baseline Array (VLBA) and the Very Large Array (VLA) that reveal that LS 5039 is resolved into bipolar radio jets emanating from a central core.

[1]Departament d'Astronomia i Meteorologia, Universitat de Barcelona, Av. Diagonal 647, E-08028 Barcelona, Spain. [2]Departamento de Física, Escuela Politécnica Superior, Universidad de Jaén, Calle Virgen de la Cabeza 2, E-23071 Jaén, Spain. [3]Max Planck Institut für Radioastronomie, Auf dem Hügel 69, D-53121 Bonn, Germany.

*To whom correspondence should be addressed. E-mail: josepmp@am.ub.es

Because LS 5039 appeared unresolved (≤0.1″) to the VLA alone, we proceeded to study this object with milliarc sec resolution using the VLBA at the frequency of 5 GHz (6-cm wavelength) on 8 May 1999. The VLA in its phased array mode, equivalent to a dish of 115-m diameter, also participated as an independent station, providing sensitive baselines with the VLBA antennas. The source 3C345 was used as a fringe-finder, whereas J1733-1304 was the phasing source for the VLA. The data were calibrated using standard procedures in unconnected radio interferometry. The resulting pattern of the observed visibility amplitudes, decaying as a function of baseline length, indicated that LS 5039 had structure at milliarc sec scales.

The final synthesis map (Fig. 1) shows that bipolar jets emerge from a central core. A de-